JCI The Journal of Clinical Investigation

γ9δ2T cell diversity and the receptor interface with tumor cells

Anna Vyborova, … , Zsolt Sebestyen, Jürgen Kuball

J Clin Invest. 2020;130(9):4637-4651. https://doi.org/10.1172/JCI132489.

Research Article | Immunology | Oncology

Graphical abstract

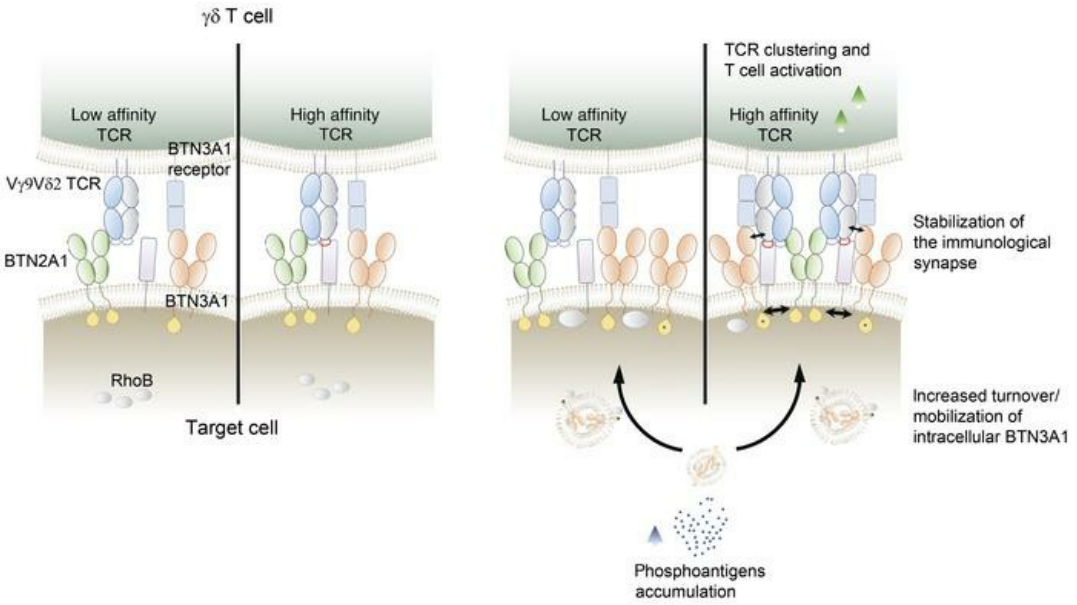

γ9δ2T cell diversity and the receptor interface with tumor cells

Anna Vyborova,[1] Dennis X. Beringer,[1] Domenico Fasci,[1] Froso Karaiskaki,[1] Eline van Diest,[1] Lovro Kramer,[1] Aram de Haas,[1] Jasper Sanders,[1] Anke Janssen,[1] Trudy Straetemans,[1] Daniel Olive,[2] Jeanette Leusen,[1] Lola Boutin,[3] Steven Nedellec,[4] Samantha L. Schwartz,[5,6] Michael J. Wester,[7] Keith A. Lidke,[7] Emmanuel Scotet,[3] Diane S. Lidke,[5,6] Albert J.R. Heck,[8,9] Zsolt Sebestyen,[1] and Jürgen Kuball[1,10]

[1]Center for Translational Immunology, University Medical Center (UMC) Utrecht, Utrecht University, Utrecht, Netherlands. [2]Centre de Recherche en Cancérologie Marseille, INSERM, Institut Paoli-Calmettes, Marseille, France. [3]Université de Nantes, INSERM, CNRS, CRCINA, LabEx IGO "Immunotherapy, Graft, Oncology," Nantes, France. [4]Structure Fédérative de Recherche en Santé François Bonamy (SFR-Santé), INSERM, CNRS, CHU Nantes, Nantes, France. [5]Department of Pathology, [6]Comprehensive Cancer Center, and [7]Department of Physics and Astronomy, University of New Mexico (UNM), Albuquerque, New Mexico, USA. [8]Biomolecular Mass Spectrometry and Proteomics, Bijvoet Center for Biomolecular Research and Utrecht Institute for Pharmaceutical Sciences, Utrecht University, Utrecht, Netherlands. [9]Netherlands Proteomics Centre, Utrecht, Netherlands. [10]Department of Hematology, UMC Utrecht, Utrecht University, Utrecht, Netherlands.

γ9δ2T cells play a major role in cancer immune surveillance, yet the clinical translation of their in vitro promise remains challenging. To address limitations of previous clinical attempts using expanded γ9δ2T cells, we explored the clonal diversity of γ9δ2T cell repertoires and characterized their target. We demonstrated that only a fraction of expanded γ9δ2T cells was active against cancer cells and that activity of the parental clone, or functional avidity of selected γ9δ2 T cell receptors (γ9δ2TCRs), was not associated with clonal frequency. Furthermore, we analyzed the target-receptor interface and provided a 2-receptor, 3-ligand model. We found that activation was initiated by binding of the γ9δ2TCR to BTN2A1 through the regions between CDR2 and CDR3 of the TCR γ chain and modulated by the affinity of the CDR3 region of the TCRδ chain, which was phosphoantigen independent (pAg independent) and did not depend on CD277. CD277 was secondary, serving as a mandatory coactivating ligand. We found that binding of CD277 to its putative ligand did not depend on the presence of γ9δ2TCR, did depend on usage of the intracellular CD277, created pAg-dependent proximity to BTN2A1, enhanced cell-cell conjugate formation, and stabilized the immunological synapse (IS). This process critically depended on the affinity of the γ9δ2TCR and required membrane flexibility of the γ9δ2TCR and CD277, facilitating their polarization and high-density recruitment during IS formation.

Introduction

Cancer immunotherapies with classical checkpoint inhibitors and CAR T cell therapies are limited by their dependency on the mutational load of the tumor and by the lack of targets for solid tumors (1). Within this context, clinical developers currently have a significant, renewed interest in γδT cells, because these cells have been reported to be broadly active against multiple solid cancers and hematological malignancies (2, 3). Although very few targets of γδT cells and their receptors have been described to date, the current understanding is that γδT cells act on early metabolic changes in cancer cells, which makes γδT cells attractive candidates to attack tumors with a low mutational load (for review see ref. 1). However, to date, most clinical trials have shown very limited clinical efficacy, particularly when using expanded γ9δ2T cells (1, 4).

We propose 2 possible causes for the lack of clinical success of adoptively transferred γ9δ2T cells in humans. First, most of the published and ongoing studies use polyclonally derived γ9δ2 T cells (1, 4). However, recent work suggests a substantial functional heterogeneity in this cell population (5). It is not clear whether this diversity affects the activity of γ9δ2T cells against cancer cells when used for adoptive immune therapies. A second obstacle might be the poor selection of patients for clinical trials, which is a consequence of the limited understanding of the targets expressed on tumors. Upon encountering the target, γ9δ2T cells are known to sense elevated phosphoantigen (pAg) levels through the small GTPase RhoB (6), which induces a joint spatial and conformational change in surface expression of CD277 (BTN3A) (6–12) via an inside-out signaling mechanism. A direct interaction between the γ9δ2T cells and CD277, involving the isoforms BTN3A1, BTN3A2, and BTN3A3, has been suggested (13). Given the homology of BTNA1, -A2, and -A3, the Abs directed

Authorship note: AV, DXB, and DF contributed equally as coauthors. ZS and JK are both senior authors.

Conflict of interest: JK is a shareholder of Gadeta. JK, ZS, DXB, AV, AJ, and EVD are authors on the following patent applications: WO 2013/147606 A1, Combinatorial gamma 9 delta 2 T cell receptor chain exchange (JK); 20170319674, Use of antibodies for enrichment of engineered T cells with exogenous immune receptors and antibodies for use in depletion of engineered T cells (JK); WO 2017/2017/212074, Novel method for identifying delta T cell (or gamma T cell) receptor chains or parts thereof that mediate anti-tumor or anti-infectious response (JK); WO 2017/212072, Human leukocyte antigen–restricted gamma delta T cell receptors (JK); 2017/62508807, Composition and methods for cell targeting therapies (ZS and JK); 2018/6044506, GABs as next generation of immune therapy (EVD, DXB, JK).

Submitted: August 12, 2019; **Accepted:** May 28, 2020; **Published:** August 4, 2020.
Reference information: *J Clin Invest*. 2020;130(9):4637–4651.
https://doi.org/10.1172/JCI132489.

against extracellular domains of BTN3A1 usually cross-recognize BTN3A2 and BTN3A3 as well (14); therefore, with CD277, we refer to all 3 isoforms. The rearrangement in CD277 architecture that induces γ9δ2T cell activation is referred to herein as CD277J (14). However, it remains highly controversial whether CD277 interacts directly with the γ9δ2T cell receptor (γ9δ2TCR) and whether additional molecules are involved (7, 8, 13, 14).

In this study, we explored the functional heterogeneity of γ9δ2T cells on a clonal level, as well as the impact of individual γ9δ2TCRs on mediating antitumor responses in relation to their CDR3 usage and the putative ligand CD277. To this end, we isolated and functionally characterized an extensive panel of single γ9δ2T cell clones, and we cloned and expressed individual γ9δ2TCR genes. By engineering αβT cells to express a defined γδ TCR (TEG) as a next generation of chimeric antigen receptor T cells (CAR-T cells), we were able to assess the functional impact of individual γ9δ2TCRs on sensing the target, in the absence of the original functional programming of the parental clone, as well as without other NK and KIR receptors usually expressed on γ9δ2T cells (2). In addition to providing a valuable tool for the molecular characterization of individual γ9δ2TCRs, the TEG concept combines the positive aspects of 2 different cell types: the memory formation and high-proliferation capacity of αβT cells and the broad antitumor reactivity of defined γδTCRs (15, 16). TEGs demonstrated the ability to distinguish between healthy and malignant leukemic stem cells (6) and thereby overcome the obstacle of leukemic stem cells that lack, e.g., NKG2D ligands (17). In addition, we have shown that TEGs eliminate primary multiple myeloma cells in a humanized bone marrow niche (18). As a result of these findings, TEGs are currently being tested in a first-in-human clinical trial (19, 20). Within this context, our current report demonstrates that the failure of previous clinical trials using polyclonal γ9δ2T cells can be partially attributed to a high frequency of γ9δ2T cells with poor tumor reactivity within healthy immune repertoires (14). In addition, after analyzing the molecular interface between cells expressing a γ9δ2TCR and CD277, we propose a paradigm shift in the model of recognition, in which the γ9δ2TCR is only critical for initiating cell conjugation, functioning as an initial signal of T cell activation and maintaining high-density immunological synapse (IS), but is not dependent on pAgs. Conversely, CD277 operates as a mandatory coactivating ligand that functions as a second signal, stabilizes conjugation and synapse formation, and is dependent on pAgs, but not on the presence of the γ9δ2TCR.

Results

Clonal γ9δ2T cell functional diversity. In order to assess the impact of clonal heterogeneity on the antitumor functional activity of the γ9δ2 T cell population in a given individual, we isolated and expanded γ9δ2 T cell clones from the peripheral blood of healthy donors. Next, we determined the in vitro antitumor reactivity of individual clones by measuring their response to the Burkitt lymphoma cell line Daudi, which can be considered a model target for studying pAg-mediated and TCR-dependent γ9δ2 T cell responses (reviewed in ref. 21). IFN-γ production was used as a readout, since the capacity to secrete IFN-γ has been shown to be a property of the whole γ9δ2 T cell compartment, regardless of the subset (5). We observed substantial variation in cytokine secretion capacity among γ9δ2 T cell clones isolated from 3 healthy donors (donors A–C), with approximately 60% of the clones being tumor reactive according to this readout (cutoff 30 pg/mL; Figure 1A). Bisphosphonates such as pamidronate (PAM) are known to boost the γ9δ2 T cell responses by inducing or enhancing CD277J (9). Consistent with these findings, in the presence of 100 μM PAM, the reactivity of the γ9δ2T cell clones was increased by 10-fold on average (median 8.1, IQR = 15.0–3.4), with more than 95% of the clones showing reactivity above the threshold when PAM was added (Figure 1A and Supplemental Figure 1A; supplemental material available online with this article; https://doi.org/10.1172/JCI132489DS1). Other Th1 spectrum cytokines measured in a subset of the investigated clones showed a high correlation with IFN-γ and with each other, indicative of a robust signature (Supplemental Figure 1, B–D). HEK293T, an additional well-characterized γ9δ2 T cell target (6, 9), elicited much lower cytokine secretion in the absence of PAM, however, in the presence of PAM, reactivity of the clones was comparable to their reactivity to Daudi cells (Figure 1, B and C).

Antitumor response of individual γ9δ2T cell clones does not correlate with clonal frequency. As little is known about functional implications of the diversity in the γ9δ2TCR repertoire, it was particularly interesting to explore the antitumor response of the individual γ9δ2T cell clones in the context of their clonotype frequencies. We selected 20 clones for TCR sequencing to track their clonotype within the original bulk population, covering the full range of clonal activities, as depicted in Figure 1A (arrows). Several clones (B2/B5, C4/C14, C7/C11/C15, C6/C9/C13) were found to express the same γ9δ2TCR, yielding a total of 16 unique clonotypes. All δ chains were unique, whereas we observed public (shared between donors) CDR3γ sequences, as well as pairing of 1 TCRγ9 with different TCRδ2 chains in the same donor (Table 1), in line with high-throughput sequencing (HTS) data reported by others (22–24). Next, we performed HTS of the complete TCRδ2 repertoires of the same donors. The prevalence of a T cell receptor δ locus (TRD) clonotype within the repertoire of a donor did not correlate with reactivity of the respective clone against Daudi or HEK293T cells, as demonstrated by the example of donor C, for whom 2 of the most prevalent TCRδ clonotypes C6/C9/C13 and C17 belonged to 3 of the most reactive γ9δ2 T cell clones isolated from this donor, whereas other prevalent clonotypes (C2/C18, C4/C14, C7/C11/C15) showed low reactivity (Figure 1, A and D). The TCRδ clonotypes of the highly reactive clones from donors A and B (B1, A3–A6) appeared to be rare, as the sequences could not be detected in the HTS data for the respective donor (Figure 1A and Supplemental Figure 1, E and F).

Functional avidity of the parental γ9δ2T cell clone does not correlate with γ9δ2TCR-mediated functional avidity. We aimed to assess whether the antitumor activity of a given γ9δ2T cell clone would associate with its functional avidity mediated by its respective TCR, as suggested by our previous study (15). We defined the binding strength of an individual receptor ligand interaction as affinity, and the combined strength governed by multiple receptor-ligand interactions as avidity. To measure the avidity of a defined γ9δ2TCR, we assessed the functional avidity of TEGs by measuring effector functions, like IFN-γ secretion, against defined targets (25–27) and compared it with the functional avidity of the parental γ9δ2T cell clone, which also harbors other

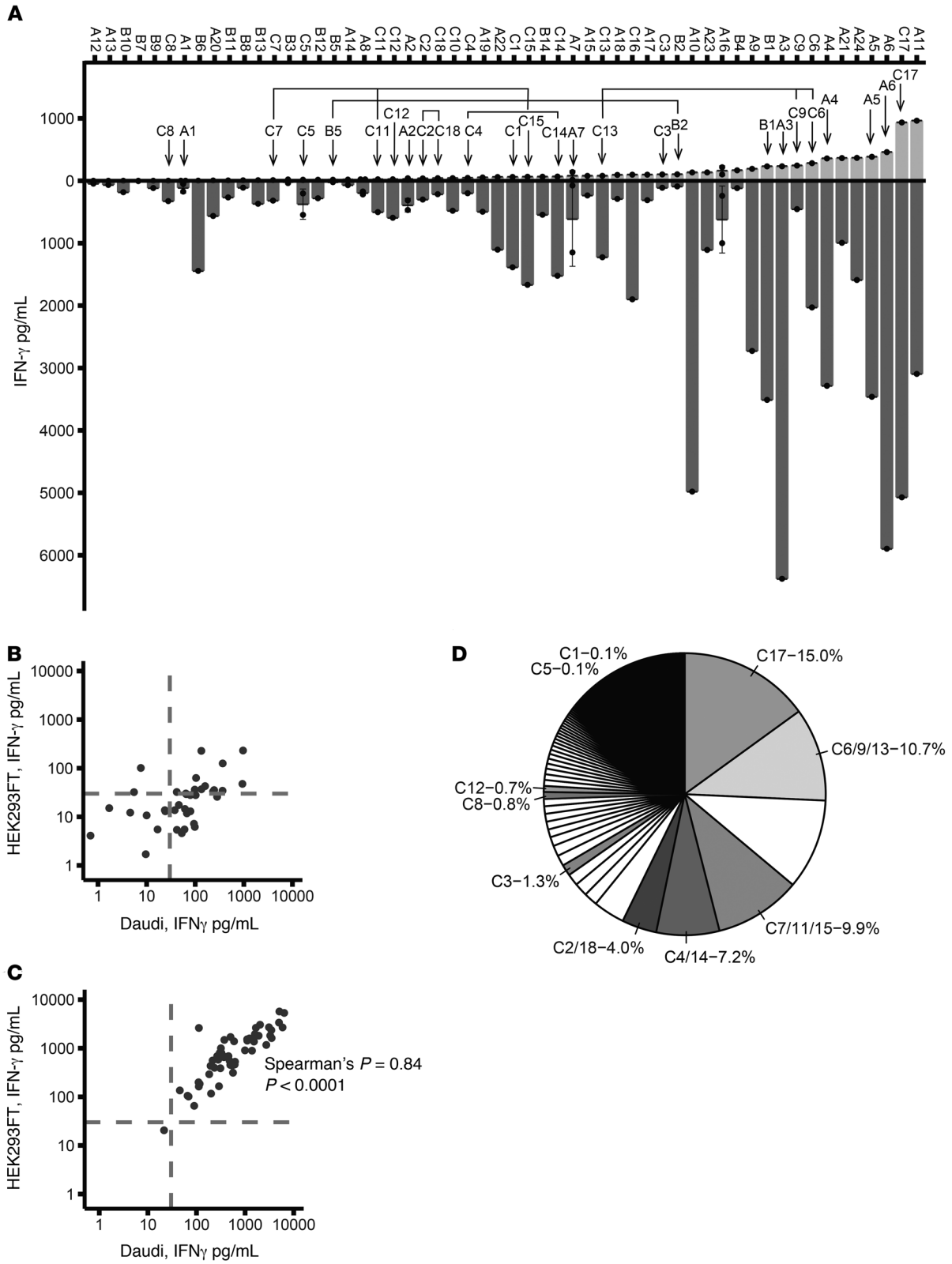

Figure 1. Antitumor reactivity of the γ9δ2 T cell clones and TRD clonotype frequencies for donor C. (**A**) Antitumor reactivity of the isolated clones assessed by IFN-γ production (n = 56). Bars represent the means of 2 to 4 biological replicates from 1 to 2 independent experiments. Arrows indicate clones with a known TCR sequence. Connecting lines indicate clones expressing the same γ9δ2 TCR. (**B** and **C**) IFN-γ production against Daudi versus HEK293T cell lines without (**B**) or in the presence of 100 μM PAM (**C**). Dashed lines represent the cutoff for reliable ELISA measurements (30 pg/mL). (**D**) Complete T cell receptor delta variable region (TRDV) repertoire for donor C. Percentages indicate clonotype frequencies. Data were filtered to exclude clonotypes with a frequency of 1 read/clonotype.

Table 1. TCR sequencing of the selected γ9δ2T cell clones

Clone ID	TCRγ	CDR3γ	CDR3γ length	TCRδ	CDR3δ	CDR3δ length
A1	TRGV9*01TRGJP*01	CALWEVKELGKKIKVF	14	TRDV2*03TRDD2*01TRDD3*01TRDJ1*01	CACDT**L**LLLGDSSDKLIF	16
A2	TRGV9*01TRGJP*01	CALW**EVQ**ELGKKIKVF	14	TRDV2*03TRDD3*01TRDJ1*01	CACDT**A**EPGGYKDKLIF	15
A3	TRGV9*01TRGJP*01	CALW**EVQ**ELGKKIKVF	14	TRDV2*03TRDD3*01TRDJ1*01	CACDA**W**GHTDKLIF	12
A4	TRGV9*01TRGJP*01	CALWEVEGLGKKIKVF	14	TRDV2*03TRDD3*01TRDJ1*01	CACDA**L**GDTGSDKLIF	14
A5	TRGV9*01TRGJP*01	CALWEAGELGKKIKVF	14	TRDV2*03TRDD3*01TRDJ1*01	CACDT**L**GALYTDKLIF	14
A6	TRGV9*01TRGJP*01	CALWEVRQELGKKIKVF	15	TRDV2*03TRDD3*01TRDJ1*01	CACDQ**L**GDPDKLIF	12
A7	TRGV9*01TRGJP*01	CALW**EVR**ELGKKIKVF	14	TRDV2*03TRDD3*01TRDJ1*01	CACDS**D**PDWGILNTDKLIF	17
B1	TRGV9*01TRGJP*01	CALWEAQVELGKKIKVF	15	TRDV2*03TRDD3*01TRDJ1*01	CACDT**P**WGIPAAQDTDKLIF	18
B2/B5	TRGV9*01TRGJ1*02	CALWEVRYYKKLF	11	TRDV2*03TRDD2*01TRDD3*01TRDJ1*01	CACDP**R**FLAWGTTDKLIF	16
C1	TRGV9*01TRGJP*01	CALW**EVR**ELGKKIKVF	14	TRDV2*01TRDD2*01TRDJ1*01	CACDP**V**PSIHDTDKLIF	15
C2	TRGV9*01TRGJP*01	CALW**EVR**ELGKKIKVF	14	TRDV2*03TRDD3*01TRDJ1*01	CACDQ**A**GGPDKLIF	12
C3	TRGV9*01TRGJP*01	CALWEVGLGKKIKVF	13	TRDV2*01TRDD3*01TRDJ1*01	CACDT**V**SGGYQYTDKLIF	16
C4/C14	TRGV9*01TRGJP*01	CALWEVSGELGKKIKVF	15	TRDV2*02TRDD2*01TRDD3*01TRDJ1*01	CACDT**L**ALGDTDKLIF	14
C5	TRGV9*01TRGJP*01	CALW**EVQ**ELGKKIKVF	14	TRDV2*02TRDD3*01TRDJ1*01	CACDL**L**APGDTSFTDKLIF	17
C6/C9	TRGV9*01TRGJP*01	CALWEVKRELGKKIKVF	15	TRDV2*02TRDD3*01TRDJ1*01	CACDT**V**VLGTGGYRDDKLIF	18
C7/C11	TRGV9*01TRGJP*01	CALW**EVR**ELGKKIKVF	14	TRDV2*01TRDD3*01TRDJ3*01	CACDM**G**DASSWDTRQMFF	16

Paired sequences of the TCRδ and -γ CDR3 regions of the selected clones. Sequences were analyzed using the IMGT/V-QUEST tool (http://www.imgt.org/IMGT_vquest/user_guide) in order to determine the identity of the germline segments. Amino acid sequences defining public TCRγ9 clonotypes (24, 45) and amino acids at "position 5" of the TCRδ2 (24) are highlighted in bold. The conserved cysteine of the V region and phenylalanine of the J region were not included when calculating the CDR3 length.

NK-like receptors (Figure 1). First, the individual γ9δ2TCRs were expressed in the absence of other receptors present on parental γδT cells in the human TCR-deficient T cell line Jurkat-76. The previously reported low functional avidity ("weak") γ9δ2TCR CTE-Cl3, high functional avidity ("strong") γ9δ2TCR CTE-Cl5, and nonfunctional length mutant 1 (LM1) that were generated by combinatorial TCR chain exchange (CTE) with the chains of the TCR G115 (15, 28) were used as an additional framework. For γ9δ2TCRs from all donors, we observed consistent differences in functional avidity, as evidenced by unequal CD69 upregulation and downregulation of the γδTCR upon stimulation with the cell line Daudi (Figure 2, A–F, and Supplemental Figure 2, A–F) in cells selected for equivalent γ9δ2TCR expression. These cells were able to overcome heterogeneous γ9δ2TCR expression from the initial bulk, and later from engineered immune cells (Supplemental Figure 2, G and H). Differences in functional avidity were even more evident in γ9δ2TCR-transduced primary αβT cells with equivalent γ9δ2TCR expression (Supplemental Figure 2, G–J), when we used IFN-γ secretion or tumor cell lysis as a readout (Figure 2, G and H), since primary T cells have a better capacity to produce cytokines and directly kill than do Jurkat cell lines (29). The outcomes of different readouts, such as CD69 upregulation for Jurkat-76, and IFN-γ secretion and tumor cell lysis for TEGs, correlated with each other, indicating that the effect was indeed due to the introduced γ9δ2TCRs with defined sequences and was not the property of a defined transduced cell (Supplemental Figure 2I).

Although responses mediated by distinct γ9δ2TCRs, such as TCR A3, correlated with the ability of the parental clone to mediate exceptionally high antitumor reactivity upon PAM stimulation (Figure 1A), functional avidity mediated through other TCRs did not correlate with the antitumor response of their parental clone. For example, the primary clones A1 and A2 showed similarly low reactivity (Figure 1A), whereas TCRs isolated from these clones mediated unequal responses in the TEG format (Figure 2, A, D, G, and H). Conversely, the TCR A5, whose parental clone showed antitumor activity in the higher range, did not differ in activation potential from the TCR derived from the clone A1. These data imply that epigenetic imprints modulate the response of primary γ9δ2T cells on a clonal level (2, 5, 30, 31). Although the functional avidity of a given γ9δ2TCR CDR3 seems to be of ambiguous relevance for the response of its parental T cell clone, we demonstrate here that γ9δ2TCR CDR3 is crucial for the antitumor activity of TEGs. In addition, our data suggest a range of affinities for different γ9δ2TCRs that do not, however, exceed a certain threshold. The assumption of these experiments would be that polyclonal γ9δ2T cells are inferior in terms of reactivity against tumor targets when compared with TEGs expressing high-affinity γ9δ2TCR. To test this hypothesis, we coincubated γ9δ2TCR CTE-Cl5–engineered immune cells and bulk γδ T cells with a variety of different tumor cell lines and with primary acute myeloid leukemia (AML) blasts. As expected, γ9δ2TCR CTE-Cl5–engineered T cells showed superior IFN-γ production in response to various tumor cells and primary AML blasts, thus outperforming bulk γδ T cells (Supplemental Figure 2, K and L).

Strength of the γ9δ2TCR-tumor interaction depends on the tumor type, number of γ9δ2TCR molecules, and the CDR3 domain of the TCRδ chain. As TEG antitumor activity was fully dependent on the γ9δ2TCR CDR3 region, we next focused on a better characterization of the molecular interface of the γ9δ2TCR with its target, by taking advantage of soluble γ9δ2TCRs. Because previous reports suggested that γδTCR multimers are a suitable tool to study γδTCR-ligand interactions (32–35), we first engineered tetram-

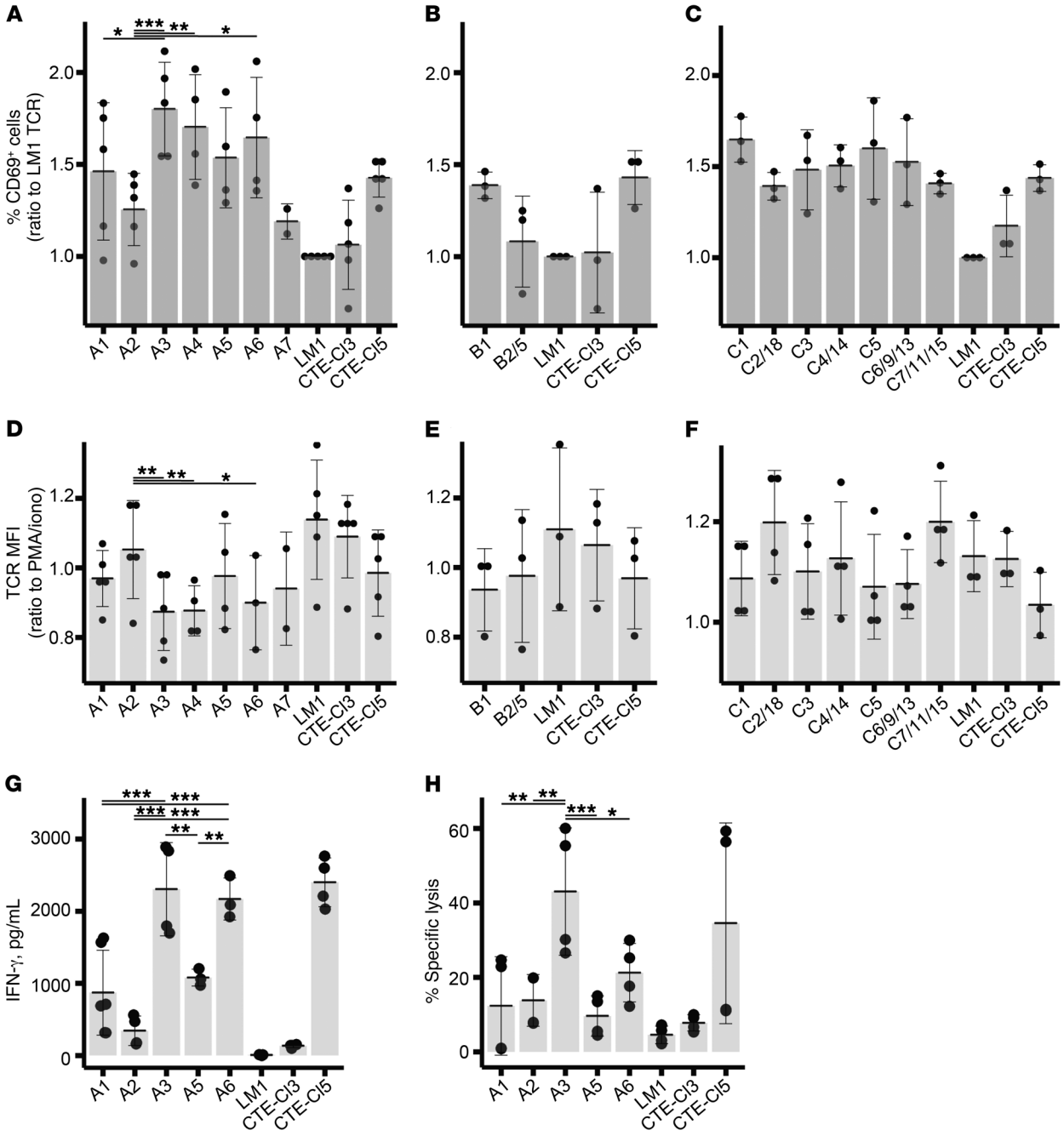

Figure 2. Functional avidity of the isolated TCRs in the TEG format. (**A**–**F**) Functional avidity of the TCRs from donors A, B, and C, next to control TCRs, transduced into the Jurkat-76 cell line (n = 2–5 from at least 2 independent transductions). (**A**–**C**) CD69 upregulation (percentage of CD69$^+$ cells) upon stimulation with the Daudi cell line, normalized to the TCR LM1 within each experiment. (**D**–**F**) TCR downregulation measured by the MFI of TCRVδ2 on Jurkat-76 cells coincubated with Daudi cells, relative to the MFI for TCRVδ2 on the same transductants treated with PMA and ionomycin (PMA/iono). Data represent mean values ± SD across experiments. (**G** and **H**) Functional avidity of the selected TCRs from donor A, next to control TCRs, transduced into primary human αβT cells. (**G**) IFN-γ production upon coincubation with Daudi cells in the presence of 100 μM PAM. Data represent mean values ± SD across 2 representative experiments. (**H**) Specific lysis of Daudi cells. Bars show mean values of 2 side-by-side biological replicates (see Supplemental Figure 2I for another representative experiment). A P value of less than 0.05 was considered significant. *P < 0.05, **P < 0.01, and ***P < 0.001, by 2-way ANOVA with Tukey's post hoc test.

ers of the γ9δ2TCRs Cl5 and the nonfunctional TCR LM1 (15), as well as the low-reactive clone A2 and the high-reactive clone A3 identified here. As controls, we included an αβTCR and a Vγ4Vδ5 TCR. In contrast to previous reports with γ9δ2TCR tetramers (33–35) and in line with the more recent suggestions of low-affinity interactions that are needed to sense target cells (6, 8), we found that γ9δ2TCR tetramers did not strongly stain the classical target Daudi, with only a slight but significant increase in MFI for the TCRs Cl5 and A3 compared with the control TCRs (Figure 3A). However, when we screened tumor cell lines other than Daudi,

such as HEK293T, γ9δ2TCR tetramers of the non-/low-reactive γ9δ2TCR LM1 and A2 had previously bound, whereas binding was further increased when using γ9δ2TCR tetramers were derived from the highly active clones, clone 5 and clone A3 (Figure 3B).

Since both Daudi and HEK293T cells are targets of the γ9δ2TCR, we addressed the question of whether raising the number of TCRs on a multimer to increase the overall avidity would result in a more pronounced staining of Daudi cells. The extracellular domains of the TCRs LM1, Cl5, A2, and A3 were coupled to streptavidin-conjugated fluorescent beads, which allowed at least 10^4 γδTCRs to be attached to the bead surface. γ9δ2TCR-coated beads were coincubated with the negative target cell line ML1 (6) and the positive target cell line Daudi. No bead conjugation to ML1 could be observed in any of the γ9δ2TCRs (Supplemental Figures 3 and 4), whereas bead conjugation to Daudi cells was dependent on the γ9δ2TCR CDR3 region (Figure 3C and Supplemental Figures 3 and 4). TCR LM1 cells showed some conjugation to Daudi cells, just like clone A2, whereas the "strong" TCRs Cl5 and A3 showed significantly higher conjugation, indicating that differences in functional avidity can be attributed to the unequal affinity of the γ9δ2TCR-ligand interaction. The pronounced differences observed on Daudi cells between the different γ9δ2TCRs were less evident, or even absent, when we used these fluorescent beads on HEK293T cells (Figure 3D). Importantly, bead staining could be blocked by an anti-γδTCR Ab (Supplemental Figure 5A), suggesting a TCR-specific interaction. Of note, we did not observed γ9δ2TCR tetramer staining or γ9δ2TCR bead staining for some of the tumors cells that have been reported to be targeted by the γ9δ2TCR (Table 2).

BTN2A1 was most recently suggested as a ligand for the γ9δ2TCR through its TCR γ chain (35, 36). First, we tested whether one of the proposed mutations in the TCR γ chain (His85Arg) (37), which has been suggested to interact with BNT2A1, could abrogate the binding of TCR multimers to tumor cells. Indeed, $\gamma9_{\text{His85Arg}}\delta2$TCR tetramers and $\gamma9_{\text{His85Arg}}\delta2$TCR-coated beads no longer bound to Daudi or to HEK293T cells (Figure 3, A–D). Next, we assessed the impact of CD277 KO and BTN2A1 KO on target cells in γ9δ2TCR tetramer binding. Although CD277 KO did not affect γ9δ2TCR tetramer binding, differences between γ9δ2TCR LM1 and Cl5 tetramers were still evident. KO of BTN2A1 completely abrogated γ9δ2TCR tetramer binding to both γ9δ2TCR LM1 and Cl5 tetramers, indicating that a high-affinity CDR3 TCRδ chain does not overcome the lack of binding through the TCR γ chain (Supplemental Figure 3A).

γ9δ2TCR target interaction does not depend on PAM, and CD277 binding does not require the γ9δ2TCR. γ9δ2TCRs have been reported to trigger T cell responses by sensing a joint spatial and conformational change in CD277 at the cell membrane of cancer cells (CD277J) that is induced by a pAg-high state of the target cell (6, 8, 9, 11). Although we demonstrated that binding of tetramers to tumor cells heavily depended on BTN2A1, TCR binding could be further modulated through PAM-induced mobility changes of CD277. Therefore, we examined whether our γ9δ2TCR-coated beads fully mimicked the mode of action of a γ9δ2TCR in interacting with its target. First, we questioned whether the pAg level fine-tunes the activation state of the γ9δ2T cell by increasing TCR-ligand interaction affinity, and thus whether binding of the γ9δ2TCR-coated beads could be modulated by PAM treatment of the target cells. Surprisingly, the addition of PAM did not change the intensity of the TCR tetramer or TCR-coated bead conjugation to either Daudi cells or HEK293T cells (Figure 3, A–D), indicating that while capturing unequal TCR affinities, TCR-coated beads do not sense the CD277J that induces γ9δ2T cell activation, and thus adding to the conflicting data on the possibility of a direct or indirect γ9δ2TCR-CD277 interaction (6–8, 13). Our observation would imply that, conversely, CD277 on a tumor cell does not need the γ9δ2TCR to bind to a T cell. Therefore, we next assessed whether the extracellular domains of CD277 interact with T cells in a γ9δ2TCR-independent manner. Tetramers of biotinylated CD277 ectodomains (CD277e) were incubated with Jurkat-76 cells, either nontransduced or transduced with γ9δ2TCR Cl5. In line with the assumption that CD277 is not the ligand for γ9δ2TCR, we observed strong CD277e tetramer and bead conjugation for both γ9δ2TCR$^+$ and γ9δ2TCR-deficient Jurkat-76 cells, but not for Daudi cells (Figure 3, E and F). Binding of CD277e-coated beads could be specifically abrogated by anti-CD277 Abs and by the introduction of a mutation proposed by Willcox et al. (37), but not by anti-γδTCR Abs (Supplemental Figure 5B). Arg44Glu in CD277e abrogated the binding of this mutant to Jurkat-76 cells (Figure 3, E and F). These observations are in line with previous reports showing interaction of soluble CD277e constructs with T cell lines and activated primary T cells (38, 39).

In summary, our data show that (a) binding of γ9δ2TCR to BTN2A1 was dominated by the TCR γ chain and was further fine-tuned by the affinity of the CDR3 region of the TCRδ chain, (b) binding of the γ9δ2TCR to tumor cells was independent of CD277 and PAM, and (c) CD277 did not require γ9δ2TCR expression for interaction with T cells.

Conjugation enhancement depends on γ9δ2TCR affinity and PAM. Our data suggest that targeting a tumor cell with a γ9δ2TCR expressed on a T cell membrane depends at least on a 2-receptor, 3-ligand interaction rather than a single-receptor, single-ligand binding event. To gain more insight into the orchestration of BTN2A1 and BTN3A1 and the γ9δ2TCR, we assessed whether binding of the TCRs to tumor cells, as opposed to conjugation of the TCR beads, would change if we used a more dynamic model that would allow flexible membrane processes and assistance of additional cell membrane molecules. This was achieved by analyzing cell conjugation between γδTCR-expressing Jurkat/MA (JurMA) cells and HEK293FT cells as targets. Similar to γ9δ2TCR bead staining, cell-cell conjugate formation correlated with TCR affinity in the absence of PAM (Supplemental Figure 6), suggesting that TCR affinity governs conjugate formation between a T cell expressing the γ9δ2TCR and a tumor cell. However, whereas PAM treatment had no effect on γ9δ2TCR-coated bead binding, it increased the number of conjugates to the levels observed for the functional γ9δ2TCRs (Supplemental Figure 6), even in the case of the nonfunctional TCR LM1. Conjugation enhancement for a nonfunctional γ9δ2TCR suggested that PAM stabilized γ9δ2TCR-independent cell conjugates, which, in the case of a functional γ9δ2TCR, might lead to a reduction of the signaling threshold and increased γ9δ2T cell activation.

BTN2A1-BTN3A1 interaction is enhanced through a PAM-dependent increase in BTN3A1 surface recycling. BTN3A1 has been proposed to be regulated by RhoB through pAg accumulation (6).

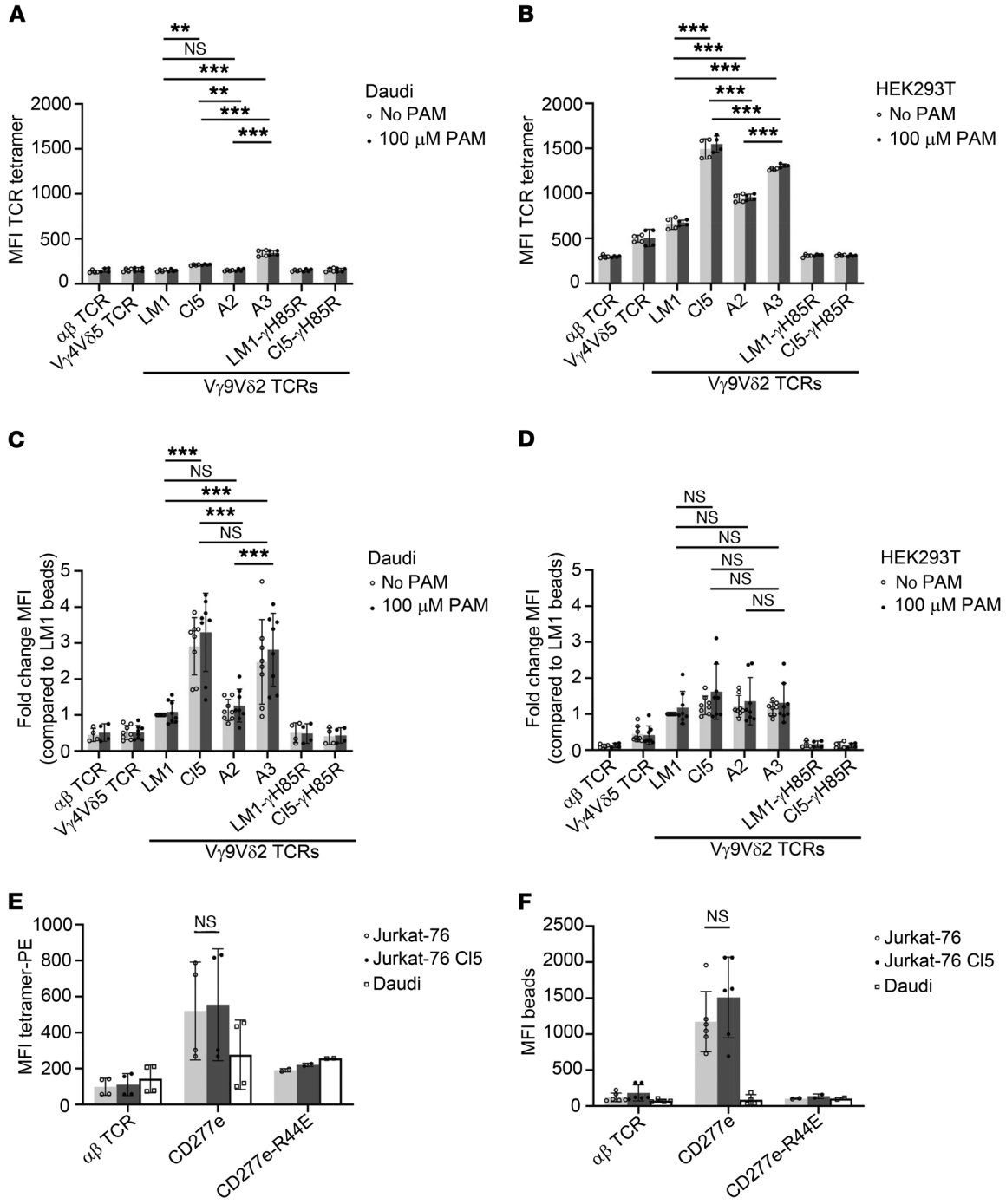

Figure 3. Staining of target and effector cells with γδTCR and CD277e multimers of increasing valency. (**A** and **B**) Results for staining of Daudi (**A**) and HEK293T (**B**) cells using fluorescent TCR tetramers (streptavidin-PE). Dots indicate the MFI values for individual FACS experiments (n = 4). (**C** and **D**) Results for staining of Daudi (**C**) and HEK293T (**D**) cells using fluorescent TCR beads (streptavidin-coated purple beads). Dots indicate the fold change in MFI values compared with LM1 (no PAM condition) in the same individual FACS experiment (n = 4, for αβTCR and Vγ9Vδ2-H85R-TCRs; n = 8 for all other TCRs). For the 100-μM PAM condition, the cells were incubated for 1 to 2 hours with PAM before staining. (**E**) Results for staining of Jurkat-76 (untransduced or transduced with Vγ9Vδ2-TCR Cl5) and Daudi cells using fluorescent tetramers containing the αβTCR control, CD277e dimers (both n = 4), or the CD277e-R44E mutant (n = 2). Dots indicate the MFI values for individual FACS experiments. (**F**) Results for staining of Jurkat-76 and Daudi cells using fluorescent tetramers containing the αβTCR control, CD277e dimers (n = 6 for Jurkat-76, n = 4 for Daudi), or the CD277e-R44E mutant (n = 2 for all cells). Dots indicate the MFI values for individual FACS experiments. For the TCR tetramer and bead staining results shown in **A**–**D**, a 1-way ANOVA followed by Dunnett's T3 multiple comparisons test was performed. A P value of less than 0.05 was considered significant. $^{**}P < 0.005$ and $^{***}P < 0.001$. For the CD277e tetramer and bead staining results shown in **E** and **F**, a 2 tailed, paired t test was performed. All statistical analysis was done using GraphPad Prism 8.3.0.

Table 2. TEG reactivity, soluble TCR tetramer and TCR bead binding, and RhoB relocalization per tumor

Tumor cell	TCR Cl5 TEG reactivity	TCR tetramer binding	TCR bead binding	RhoB relocalization
ML-I	–	–	–	–
AML 4 (primary blasts)	–	–	–	–
K562	+	+	+	+
HEK293T	+	+	+	–
Daudi	+	–	+	–
AML 1 (primary blasts)	+	–	–	+
AML 2 (primary blasts)	+	–	–	+
AML 7 (primary blasts)	+	–	–	+

TCR Cl5 TEG reactivity against a panel of tumor cell lines or patient-derived primary blasts was determined using INF-γ ELISA, tetramer and bead-binding assays were performed using TCR Cl5 as described in Figure 3, RhoB relocalization was determined by immunofluorescence staining for RhoB, and localization was analyzed using conformal microscopy as described previously (6).

However, RhoB relocalization alone did not fully explain the recognition of a tumor cell through a γ9δ2TCR (Table 2). To obtain additional insights into the regulation of BTN3A1 after pAg accumulation, we generated a stable cell line expressing FLAG-tagged BTN3A1 (Supplemental Figure 7), and to search for additional PAM-dependent interaction partners, we analyzed changes in the interactome of BTN3A1 with or without PAM treatment. Affinity purification coupled with mass spectrometry (AP-MS) from the cells expressing FLAG-BTN3A1 revealed a strong enrichment of BTN2A1 in the FLAG immunoprecipitates after PAM treatment (Figure 4A). This finding was confirmed by coimmunoprecipitating FLAG-BTN3A1 and HA-BTN2A1 (Figure 4C) and suggested that the accumulation of pAgs significantly enhanced the interaction or targeting to the same membrane domain of BTN3A1 and BTN2A1. By performing a gene ontology (GO) functional enrichment analysis of the proteins significantly enriched in the FLAG-BTN3A1 immunoprecipitates after PAM treatment, we found an enrichment of proteins targeted to cellular membranes, including the endoplasmic reticulum and the plasma membrane, and to biological processes associated with these compartments and vesicle trafficking (Figure 4B). This result is consistent with the reported subcellular localization of BTN3A1 (6) and suggests that the accumulation of intracellular pAgs enhances BTN3A1 targeting to cellular membranes. To test whether PAM enhances recruitment to the plasma membrane of CD277, we evaluated the CD277 surface expression on K562 cells treated with PAM for 5 hours after supplementing with anti–CD277–Alexa Fluor 647 Ab during the entire treatment. The PAM treatment resulted in a modest increase in CD277 surface levels compared with levels on untreated cells (Figure 4D). However, this result may have been influenced by the differential response of the different CD277 isoforms to the PAM treatment and by the inability to specifically evaluate the surface expression of endogenous BTN3A1. Nonetheless, this increase in CD277 surface levels was completely abolished once cells were treated with monensin, a known inhibitor of vesicle trafficking, suggesting that PAM influenced not necessarily the overall membrane expression but rather the recycling of surface BTN3A1. To further evaluate the contribution of the intracellular pool of CD277 to the γ9δ2TCR-dependent recognition, we evaluated the response of bulk Vδ2$^+$ γδ T cells to K562, preincubated with a control or anti-CD277–blocking Ab before or during PAM treatment. Although the anti-CD277–blocking Ab (clone 267-21f8.19) completely prevented target cell recognition when present throughout the PAM treatment, washing the Ab away before the treatment resulted in at least 50% recovery of target cell recognition by bulk Vδ2$^+$ γδ T cells (Figure 4E) and TEGs (Supplemental Figure 8). We confirmed this finding by preincubating target cells with inhibitors of vesicle trafficking such as brefeldin A or monensin, both of which were effective in preventing γ9δ2TCR Cl5 TEG–mediated recognition of the target cell (Figure 4F). These data suggest that the BTN2A1-BTN3A1 interaction or plasma membrane cotargeting is enhanced by PAM and is dependent on an increase in BTN3A1 surface recycling.

TCR affinity dictates the recruitment of a γ9δ2TCR toward the late IS. Next, we assessed whether formation of the late IS, a prerequisite for full T cell activation (40), depends on γ9δ2TCR affinity or PAM treatment. To address this question, we quantified accumulation of the γ9δ2TCRs to the contact area between tumor cells and T cells, relative to T cell membrane areas distant from the synapse (Figure 5, A and B). Synapse enrichment was significantly higher for the TCR CTE-Cl5 compared with the TCRs CTE-Cl3 and LM1 in the case of target cells that were not subjected to PAM treatment (Figure 5A). Even though T cells expressing a nonfunctional TCR LM1 showed an increase in conjugate formation upon PAM treatment (Supplemental Figure 6), this TCR did not enrich in the IS, even when tumor cells were treated with PAM (Figure 5A). PAM treatment did not further enhance polarization of the high-affinity CTE-Cl5 TCR to the IS and only significantly increased accumulation of the low-affinity TCR CTE-Cl3 in the synapse. This finding implies that TCR affinity dictates the recruitment of a γ9δ2TCR toward the late IS and that, in the case of a low-affinity TCR, PAM treatment can boost this recruitment by stabilizing the IS via CD277.

We investigated whether PAM might influence recruitment of a given γ9δ2TCR toward the IS through changes in CD277 clustering on the tumor cell. To explore this possibility, we treated HEK293 cells stably expressing the BTN3A1 isoform linked to EmGFP with either PAM or agonist and antagonist anti-CD277 Abs (clones 20.1 and 103.2, respectively) and analyzed the cells by confocal microscopy. The number and size of BNT3A1-EmGFP clusters in the cell membrane were similar in all conditions (Figure 5C), suggesting no

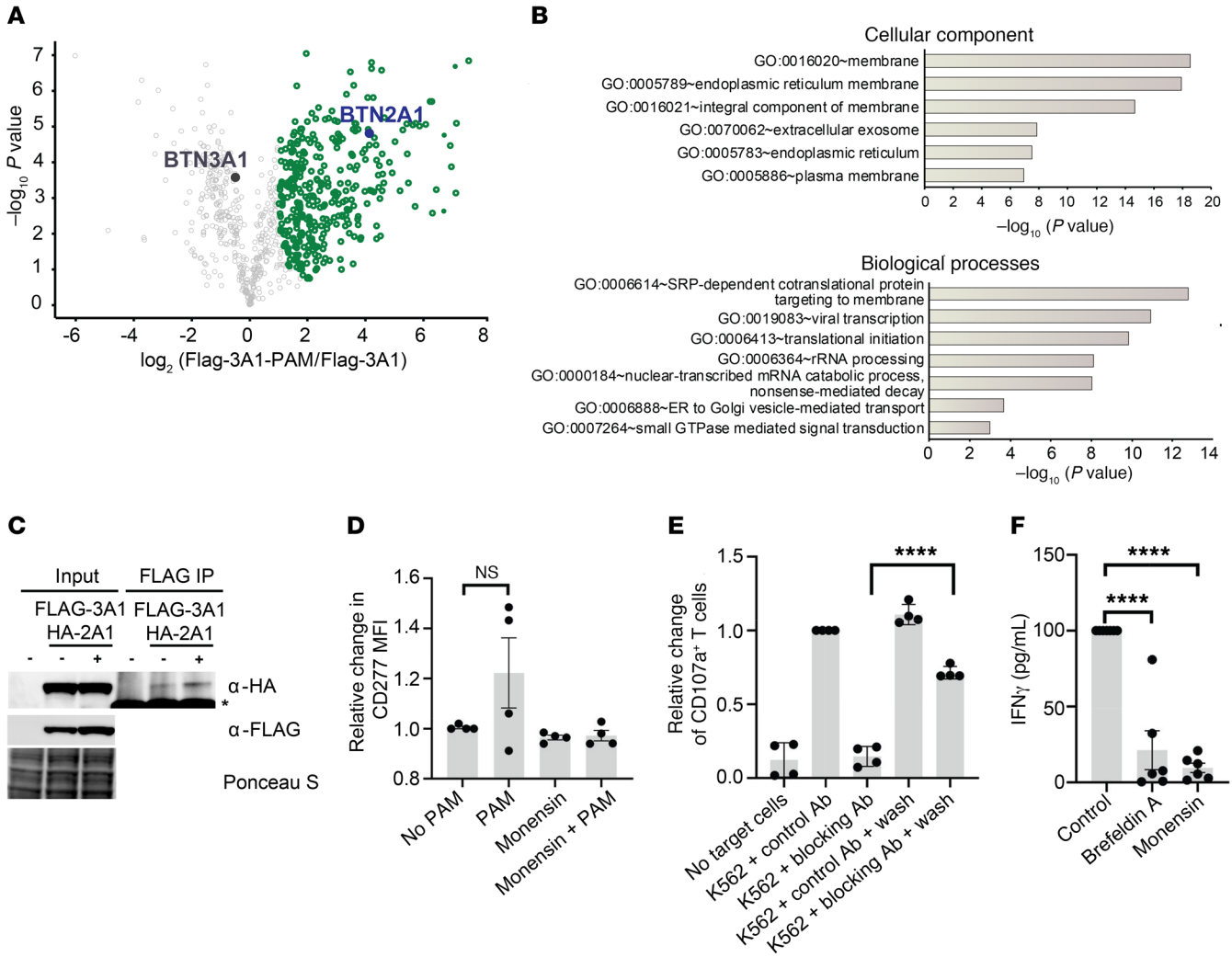

Figure 4. PAM treatment alters the interactome of BTN3A1 and the role of BTN3A1 turnover or the pAg-dependent Vγ9Vδ2 T cell activation. (**A**) Volcano plot shows the *P* values versus the difference in $\log_2$ protein intensities (proteins coenriched with BTN3A1 under the different treatment conditions). BTN2A1 coeluted with BTN3A1 after PAM treatment. The proteins significantly enriched after PAM treatment are highlighted in green, BTN2A1 in blue, and BTN3A1 in gray. (**B**) GO enrichment analysis of the proteins significantly coenriched with BTN3A1 after PAM treatment using the Database for Annotation, Visualization, and Integrated Discovery (DAVID). (**C**) Coimmunoprecipitation from HEK293T-CD277–KO cells transiently transfected with FLAG-BTN3A1 and HA-BTN2A1. PAM treatment enhanced the association between BTN3A1 and BTN2A1. The asterisk indicates the IgG heavy chain contaminant. Data are representative of 3 independent experiments. α, anti. (**D**) Results for CD277 stainings of K562 cells cultured for 5 hours under different conditions in the presence of anti–CD277-AF647 Ab. Dots indicate the relative MFI values for individual FACS experiments. Data indicate mean values ± SD. (**E**) Results for CD107a staining of Vδ2 T cells cocultured with K562 cells treated with 100 μM PAM and preincubated for 45 minutes with a control Ab or a CD277-blocking Ab (clone 267-21f8.19) before starting the treatment or retained throughout the treatment. Dots indicate the relative changes in $CD107a^+$ T cells for individual FACS experiments. Data indicate mean values ± SD. A *P* value of less than 0.05 was considered significant. $^{****}P < 0.0001$, by 2 tailed, unpaired *t* test. (**F**) IFN-γ release of TCR Cl5 TEGs cocultured with HEK293T cells pretreated with either monensin or brefeldin A and washed extensively before coculture. Data indicate mean values ± SD. A *P* value of less than 0.05 was considered significant. $^{****}P < 0.0001$, by 1-way ANOVA, defining comparisons between the treatments and the control sample.

increase in CD277 cluster size induced by stimulation of the tumor cells with the activating Ab or PAM. However, the lateral resolution of the confocal microscope is limited to approximately 300 nm, and we may therefore have missed smaller clusters.

To examine CD277 organization at the nanoscale in the presence or absence of PAM stimulation, we performed direct stochastic optical reconstruction microscopy (dSTORM), a localization-based super-resolution imaging technique that provides approximately 20-nm resolution (41). CD277 molecules were labeled with AF647-CD277 Ab, and super-resolution images were acquired at the basal membrane of HEK293T cells (Supplemental Figure 9). We found predominantly random CD277 distribution in both control and PAM-treated HEK293T cells, as Hopkins statistic values (H values) were centered around 0.5 (Figure 5D). By comparing the distribution of the localizations per cluster, we further confirmed that neither PAM treatment nor preincubation with agonist anti-CD277 20.1 Ab dramatically changed the spacing between CD277 molecules (Figure 5E and Supplemental Figure 9, A and B), whereas EGF treatment as a positive control resulted in enrichment of clusters of EGFR in the membrane of

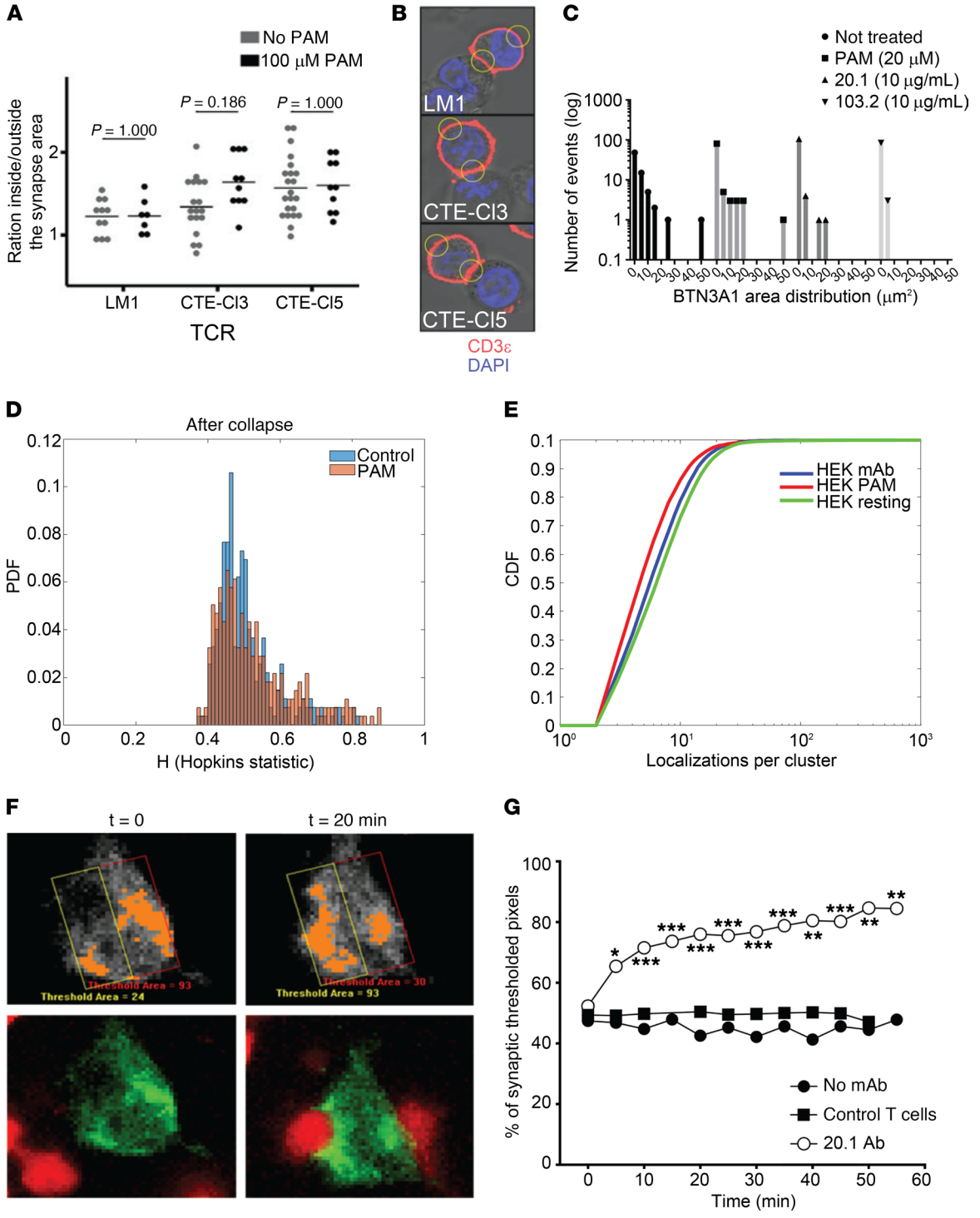
A
No PAM
100 μM PAM
P = 1.000
P = 0.186
P = 1.000
Ration inside/outside the synapse area
LM1
CTE-CI3
CTE-CI5
TCR
B
LM1
CTE-CI3
CTE-CI5
CD3ε
DAPI
C
Not treated
PAM (20 μM)
20.1 (10 μg/mL)
103.2 (10 μg/mL)
Number of events (log)
BTN3A1 area distribution (μm²)
D
After collapse
Control
PAM
PDF
H (Hopkins statistic)
E
HEK mAb
HEK PAM
HEK resting
CDF
Localizations per cluster
F
t = 0
t = 20 min
Threshold Area = 24
Threshold Area = 93
Threshold Area = 30
Threshold Area = 93
G
% of synaptic thresholded pixels
No mAb
Control T cells
20.1 Ab
Time (min)

Figure 5. Target cell-surface distribution of BTN3A1 with and without γ9δ2T cell engagement. (**A**) Enrichment of the TCR in the IS was quantified as the ratio between CD3ε-AF647 Ab signal intensity inside versus outside the synapse area. Analysis was done on at least 7 independent T cell–tumor cell conjugate images (representative images are shown in **B**). Significance was determined by 2-way ANOVA with Mann-Whitney *U* post hoc analysis. A *P* value of less than 0.05 was considered significant. Dots represent individual images, and bars represent the median values. (**B**) Representative images of the TEG–tumor cell conjugates and the regions of interest (ROIs) used for quantification. Original magnification, ×63. (**C**) Topology of BTN3A1 molecules: the number of fluorescence events on the cell membrane (BTN3A1-EmGFP) was classified according to the cluster size based on confocal microscopic analysis of HEK293T cells stably expressing BTN3A1-EmGFP (n = 15). (**D**) Histogram comparing the Hopkins statistic (H) of BTN3A1 clustering for control and PAM-treated cells, imaged using dSTORM. A total of 275 ROIs across 10 cells were analyzed, and the probability distribution function (PDF) for H was plotted. (**E**) Cumulative distribution function (CDF) for the nearest neighbor distances (NNDs) for control-treated (HEK resting, green), PAM-treated (HEK PAM, red), and 20.1 Ab–treated (HEK mAb, blue) samples. The CDF plots presented are read as follows: the curve furthest to the right for high values of the CDF represent data that tend to have greater localizations per cluster compared with the curves on the left. (**F**) Example of BTN3A1-EmGFP polarization to the IS in the presence of 20.1 Ab. Threshold area boxes were used to calculate the percentage of synaptic threshold pixels at time point 0 (left) and 20 minutes after T cell conjugation (right, upper). The lower panel shows target cells (green) and T cells (red) at corresponding time points. Original magnification, ×20. (**G**) Synaptic BTN3A1-GFP polarization measured on HEK293T cells following engagement with primary γ9δ2T cells with or without 20.1 Ab, NKT cells served as a control. n = 30 BTN3A1-GFP cells analyzed for each condition across 3 experiments. A *P* value of less than 0.041 was considered significant. $^{*}P < 0.041$, $^{**}P < 0.0041$, and $^{***}P < 0.00041$, by 2-way ANOVA with Bonferroni's post hoc correction for multiple comparisons.

HEK293T cells overexpressing EGFR (42) in the same experimental setting (Supplemental Figure 9C). These results are consistent with CD277 existing primarily as randomly distributed molecules in the plasma membrane of the isolated tumor cells in both pAg-low and pAg-high states. Importantly, when coincubating the same target cells with γ9δ2T cells, we detected a significant accumulation of BTN3A1-EmGFP within the IS in the presence of the activating 20.1 Ab. NKT cells targeting HEK293T cells but lacking a γ9δ2TCR did not induce BTN3A1-EmGFP accumulation at the IS. Accumulation of BTN3A1 molecules was significant 5 minutes after T cell conjugation (Figure 5, F and G).

Discussion

There has been a resurgence of interest in γ9δ2T cell therapies and medicinal products based on receptors extracted from γ9δ2T cells (1–3, 14). To overcome recent failures of clinical implementation, our data advocate for a substantial reduction of the high diversity usually observed in healthy γ9δ2T cell repertoires for experimental and, even more important, therapeutic purposes. In addition to functional diversity, we observed heterogeneity in γ9δ2TCR affinities, which, however, did not always correlate with the antitumor activity of the parental clone. In stark contrast to the current understanding of the mode of action, our data imply a 2-receptor, 3-ligand system, in which binding of the γ9δ2TCR to BTN2A1 is the major initiating event of the IS formation, and highlight the importance of the variable domain of the TCR γ chain between the CDR2 and CDR3 regions for the first contact. Our data also emphasize the crucial role of the affinity mediated through the CDR3 region of the TCRδ chain, though the interaction of this domain with its binding partner has yet to be defined. In addition, CD277 was subsequently recruited to the IS for further stabilization in a pAg-dependent manner and ultimately ended up in close proximity to BTN2A1. This recruitment included the accumulation of CD277 from other membrane sites that were not in contact with the target, as well as the mobilization of intracellular CD277.

Both TCR CDR3 region diversity (15, 43) and variable expression of an array of other nonrearranged activating and inhibitory receptors (2, 30, 44) have been reported to contribute to functional heterogeneity within the γ9δ2T cell population. We provide formal evidence that this diversity also substantially affected the antitumor activity of γ9δ2T cells by highlighting the large variation in γ9δ2T cell antitumor reactivity on a clonal level, and further demonstrating unequal TCR affinities harbored within the diverse γ9δ2TCR repertoires. The reduced diversity within 1 donor and interindividual variations can most likely be attributed to a phenomenon called "repertoire focusing." TCR repertoire focusing, or skewing toward a limited number of dominant clonotypes, has been described for both $V\delta2^{+}$ and $V\delta2^{-}$ subsets (22–24, 45). Major changes to the TCRδ2 repertoire happen postnatally, with a significant shift in dominant clonotypes according to their pAg reactivity (24), which is presumably antigen driven and strongly implies involvement of the γ9δ2TCR in constructing the functional landscape of γ9δ2T cells during ontogeny. Skewing of the repertoire toward a few dominant clonotypes implies a certain functional benefit in the conditions of selective pressure (46), however, although we observed highly focused repertoires, we did not find a correlation between clonotype frequency and antitumor functional potential of the respective T cell clone or its TCR in our experimental system. The impact of TCR affinity on maturation of the polyclonal γ9δ2T cell repertoire thus remains uncertain. The plausible explanation could be that clonotypic expansions, as a reflection of the microbial stimulation history of an individual after birth (24), either are not TCR driven or do not necessarily represent the functional hierarchy of the clonotypes when measuring in vitro tumor–induced activation.

Though the observed functional heterogeneity mediated through different γ9δ2TCRs emphasizes the possibly adaptive character of the γ9δ2T cell response, the fact that we did not always observe a direct correlation between functional avidity of the TCR and reactivity of its parental clone implies a significant "shaping" of individual γ9δ2T cell clones by other surface or cytoplasmic factors, which might be induced by microbial challenge, but may not be further involved in antitumor responses. Repertoire shifts (47) favoring expansion of potentially poorly or nontumor-reactive clones might explain a more than 15-year history of failure when using polyclonal and phenotypically diverse γ9δ2T cells to treat cancer (4), arguing for more precisely targeted applications to improve clinical outcomes when using γδT cells (14, 31, 44, 48–50).

Regardless of the role of the affinity of an individual γ9δ2TCR within the environment of its parental γδT cell, the TCR-mediated function is intriguing in the context of next-generation TCR and CAR-T therapies (3), since exploiting a γ9δ2TCR outside of its parental clone overcomes potentially unfavorable clonotypic

or phenotypic features (6, 15, 18, 51, 52). In the current study, we demonstrate intrinsic differences in γ9δ2TCR-mediated reactive potential that dictate the antitumor response of T cells engineered to express a defined γδTCR (TEGs). None of the newly isolated γ9δ2TCRs, however, exceeded the functional avidity mediated by the previously described model TCR clone 5 (15) in the TEG format, suggesting that a natural affinity ceiling is also relevant for the γ9δ2TCR, as reported for αβTCRs and Abs (53). The possible molecular determinants of γ9δ2TCR-mediated reactivity have been the focus of extensive studies, and "position 5" of the CDR3δ (ImMunoGeneTics [IMGT] position 109), which is known to have highly conserved hydrophobic amino acids, was shown to determine the γ9δ2TCR-mediated response (54). In our data set, low or absent γ9δ2TCR-mediated reactivity was associated with amino acids A, G, R, or D at this position (TCRs A2 and C2, C7/C11, B2/B5, A7; see Table 1) rather than with the highly prevalent amino acids L, V, or W. In our study, the amino acid proline (TCR B1), reported earlier to confer nonreactivity to pAgs (54), mediated reactivity comparably to CDR3δ sequences featuring L/V/W at this position.

When entering the clinic with medicinal products based on γ9δ2TCRs, it is, of course, of utmost importance to select for patients with a high likelihood of response and to thus be able to characterize the expression of the γ9δ2TCR target. However, the poor description of the mode of action of γ9δ2TCR-expressing T cells makes it challenging to develop tools that allow for robust detection of the target. To address this challenge, we developed γ9δ2TCR tetramers and γ9δ2TCR-coated beads as tools. Surprisingly, γ9δ2TCR-coated bead conjugation was independent of pAgs and did not fully mimic the currently understood mode of action, a finding that may fuel the ongoing debate as to whether CD277 directly interacts with the γ9δ2TCR (6–8, 13, 55). By using CD277-KO tumor cells and our staining tools, we demonstrate that binding of the γ9δ2TCR to its target can occur in the absence of CD277. In line with most recent reports (35, 36), our data indicate the crucial role of BTN2A1 as the first contact. However, we extended these findings by demonstrating that not only the variable framework region of the TCR γ chain but also the CDR3 region of the TCRδ chain is important in modulating the first contact between the γ9δ2TCR and its target. In addition, we demonstrate that this initiating event can substantially differ between different tumor targets, as implied by our observation that excellent tumor targets of a γ9δ2TCR like Daudi, which were barely stained with γ9δ2TCR tetramers, could bind to γ9δ2TCRs when coupled to beads. We also identified tumor cells such as primary AML blasts, which could not be stained at all with these tools, highlighting the question of whether such static tools can truly mimic the γ9δ2TCR-ligand interaction. When using γ9δ2TCR multimers alone, it is challenging to identity patients suitable for γ9δ2TCR-based immune therapies.

We therefore focused on the second key partner, CD277, and show that CD277e binding to a T cell did not depend on the γ9δ2TCR. Our data support a 2-receptor, 3-ligand model, in which the γ9δ2TCR mediates the first contact with BTN2A1 and a second ligand, followed by a third step involving CD277, which serves as an essential coactivating ligand and most likely interacts with another receptor to stabilize cell-cell vicinity and consequently reduce the γ9δ2TCR-mediated activation threshold. Unequal γ9δ2TCR affinities further modulate the magnitude of the IS formation and T cell activation. The interaction partner of the CDR3 region of the TCRδ chain has yet to be defined (Figure 6).

We also elucidated the important role of cellular trafficking of CD277. After contact with the T cell, CD277 is recruited from the noninteracting cell membrane parts to the IS and relies on intracellular CD277, which then associates with more membrane-bound molecules, indicating a higher membrane recycling of CD277. In line with our previous observation, this second step is most likely coordinated by RhoB (6). The ability of a target cell to use the intracellular storage pools most likely depends on that cell's ability to activate RhoB-dependent pathways, so that RhoB is then located at the end of the process, next to the membrane, and induces changes in membrane mobility and conformation for CD277 (6). Juxtamembrane enrichment of RhoB could serve as part of an algorithm to assess the susceptibility of a tumor cell to γ9δ2TCR-based immune therapies (6). However, RhoB does not fully describe the target, as the most prominent γ9δ2TCR target, the Daudi cell, does not show the typical juxtamembrane enrichment of RhoB (6), implying that this mechanism is only part of the recognition process.

The final question is how to characterize the previously reported pAg-induced joint changes in membrane mobility and conformation of CD277 (6, 7, 9) and their role in γ9δ2TCR-induced T cell activation in the context of these new insights. In our experimental data set, PAM treatment did not induce changes in CD277 clustering when the surface distribution of CD277 was studied on HEK293T cells alone. However, we found increased membrane expression and active accumulation of the BTN3A1-EmGFP molecules in the contact area with the T cell, suggesting that prior formation of the early synapse through the γ9δ2TCR and its ligand was required. A PAM-induced decrease in membrane mobility of CD277 (6, 9) could facilitate the formation of heterogeneous clusters, including CD277 and the γ9δ2TCR ligand, allowing both molecules to interact with their cognate receptors on T cells within the IS. Candidate binding partners for CD277, one of which is the lymphotoxin β receptor, are currently being studied (56). Another intriguing and still-open question is whether an alternative model of dual γδTCR-mediated reactivity, as described recently for mouse Vγ7$^+$ and human Vγ4$^+$ TCRs (57), could explain the apparent "uncoupling" phenomena observed in this study. In this case, existing data on the expression of the CD277 receptor on cells of myeloid lineage and B cell lines (38) would argue for a multitude of potential binding partners for CD277. Therefore, to increase the likelihood of a positive signal in clinical studies, positive staining of the tumor with γ9δ2TCR tetramers or beads as well as identification of the characteristic distribution of RhoB (6) predictive of CD277J should assist with patient selection, as long as the crucial receptor-ligand interface has not been unambiguously identified.

In summary, we demonstrate a large variation in antitumor reactivity of primary γ9δ2T cell clones. Activity against cancer cells was not associated with clonal frequency of γ9δ2T cell clones within the repertoire, which resulted in only a small fraction of γ9δ2T cell clones that were strongly reactive against cancer cells. In addition, we propose a paradigm shift in the mode of action. Our data imply a 2-receptor, 3-ligand activation model for the description of the target-receptor interface, in which the interaction of the γ9δ2TCR with BTN2A1 is mediated by the TCR γ chain,

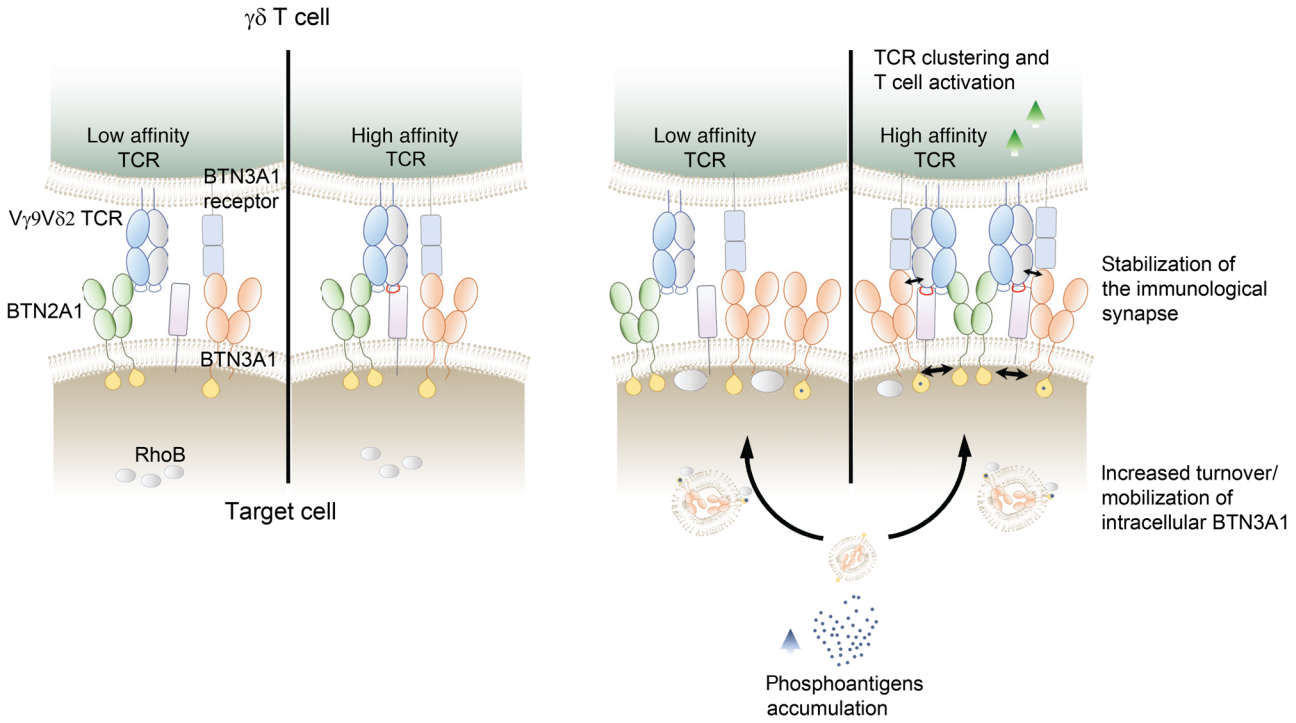

Figure 6. A 2-receptor, 3-ligand model for tumor cell recognition by γ9δ2TCR-expressing cells. While the region between CDR2 and CDR3 of the TCR γ chain (blue) directly binds to BTN2A1 on tumor cells as a major initiating event, the CDR3 region of the TCRδ chain most likely interacts with an additional, currently unknown ligand (purple) and modulates the strength of the interaction with the tumor cell. The interaction with the second ligand through the TCRδ chain critically depends on the affinity mediated via its CDR3 region. This first process is pAg independent (left). Full activation of γ9δ2TCR$^+$ T cells is only achieved, however, when BNT3A1 is recruited in a pAg-dependent manner through RhoB to the IS for further stabilization, where BTN3A1 comes into close proximity to BTN2A1. This recruitment of BTN3A1 includes the accumulation of BTN3A1 from other membrane sites that are not in contact with the target, as well as the mobilization of intracellular BTN3A1 (right). The ligand of BTN3A1 has not yet been identified.

as recently reported (35, 36). Subsequently, the CDR3 region of the TCRδ chain binds a second binding partner in a pAg-independent manner. However, the true interaction partner of the CDR3 region of the TCRδ chain has yet to be defined. The importance of this interaction was outlined by our observations that T cell conjugation, IS formation, and full T cell activation could be modulated by different affinities of the CDR3 region of the TCRδ chain. As a third event, CD277 was recruited to the IS and fixed via a RhoB-mediated mechanism. However, it is unlikely that CD277 interaction relied on the γ9δ2TCR and was mediating the pAg-dependent component via inside-out signaling, which had as a final event not only fixation of CD277 but also its close contact with BTN2A1, thereby providing the second essential coactivating signal. We believe our data pave the way for pursuit of the next ligand and have important implications for ongoing experimental and clinical efforts when exploring the use of γ9δ2T cells and their receptors for cancer immunotherapies.

Methods

Peripheral blood from anonymous healthy donors was purchased from the Dutch blood bank. γ9δ2T cells were single-cell sorted, expanded using a rapid expansion protocol (16), and tested functionally by overnight incubation with the tumor cell lines. Cytokine levels were subsequently measured in the supernatant using ELISA and/or Luminex assay. The sequences of the γ9δ2TCRs were determined by Sanger sequencing, ligated into retroviral vectors, transduced into Jurkat-76 or human primary αβT cells, and, like the primary γ9δ2T cell clones, functionally tested.

The sequences of the extracellular domains of the model γ9δ2-TCRs (15, 28) and CD277 were ligated into pBullet vectors, expressed as soluble biotinylated proteins in Freestyle 293-F cells, and coupled with streptavidin-phycoerythrin (streptavidin-PE) to generate sTCR-CD277e tetramers and dextramers (58), or with streptavidin-conjugated microspheres. The fluorescent multimers were incubated with the target cells, and conjugation was measured by FACS. More detailed information on the methods, including HTS of the TCRδ chain, cell-cell conjugation assays, confocal and super-resolution imaging, videomicroscopy, and statistical analyses, can be found in the Supplemental Methods (59–66).

HTS data. The raw HTS data were deposited in the NCBI's Sequence Read Archive (SRA) database (SRA PRJNA631458).

Resources and reagents. Requests for resources and reagents should be directed to the corresponding author.

Study approval. AML blood samples were collected from the biobank of the UMC Utrecht in accordance with good clinical practices and Declaration of Helsinki principles. All patients provided consent prior to storage of their blood samples in the biobank (TCBio 16-088). This study was approved by TCBio 16-088, UMC Utrecht (Utrecht, Netherlands).

Author contributions

AV, DXB, ES, ZS, and JK designed the study. AV, DF, DXB, EVD, LK, FK, JS, ADH, LB, SN, TS, and ZS performed the experiments. AJ

and AV analyzed the HTS data. KAL, MJW, SLS, and DSL provided methodology and analyzed the super-resolution microscopy data. AJRH, DO, and JL provided reagents and intellectual input. ZS and JK supervised the project. AV, DXB, DSL, ZS, and JK wrote the manuscript. All authors provided critical review and discussions.

Acknowledgments

We thank the staff of the Flow Core Facility and the Multiplex Core Facility at UMC Utrecht and the MicroPICell cellular and tissue imaging core facilities at CRCINA, Nantes, SFR F. Bonamy, and the University of Nantes for their expert assistance. We thank Erin Adams (University of Chicago, Chicago, Illinois, USA) for providing the CD277-KO HEK293T cell line and Halvard Boenig (Institute for Transfusion Medicine and Immunohematology, Goethe University, Frankfurt AM Main, Germany) for providing feeder cells. We thank Rachael Grattan, Aubrey Gibson, and David Schodt for help with the sample preparation and super-resolution imaging. Funding for this study was provided by grants ZonMW 43400003 and VIDI-ZonMW 917.11.337, UU 2013-6426, UU 2014-6790, and UU 2015-7601 and Gadeta (to JK), UU 2018-11393 (to ZS and JK), Marie Curie 749010 (to DXB), NIH grants R01GM100114 (to DSL), P50GM085273 (to the New Mexico Spatiotemporal Modeling Center), and P30CA118100 (to the UNM Comprehensive Cancer Center). DF and AJRH acknowledge financial support from the NWO-funded Netherlands Proteomics Centre through the National Road Map for Large-scale Infrastructures program X-Omics (project 184.034.019). ES and LB are supported by grants from INSERM, CNRS, Université de Nantes, FRM (DEQ20170839118), and Ligue Contre le Cancer AO GO2019 (Côtes d'Armor, Association pour la Recherche contre le Cancer (PJA20191209404). This work was realized in the context of the LabEx IGO program, which is supported by the French National Research Agency Investissements d'Avenir.

Address correspondence to: Jürgen Kuball, Laboratory of Translational Immunology, University Medical Center Utrecht, Utrecht University, 3584 CX Utrecht, Netherlands. Phone: 31.88.755.7230; Email: j.h.e.kuball@umcutrecht.nl.

1. Sebestyen Z, Prinz I, Déchanet-Merville J, Silva-Santos B, Kuball J. Translating gammadelta (γδ) T cells and their receptors into cancer cell therapies. *Nat Rev Drug Discov*. 2020;19(3):169–184.
2. Scheper W, Gründer C, Straetemans T, Sebestyen Z, Kuball J. Hunting for clinical translation with innate-like immune cells and their receptors. *Leukemia*. 2014;28(6):1181–1190.
3. Bouchie A, DeFrancesco L, Sheridan C, Webb S. Nature Biotechnology's academic spinouts of 2016. *Nat Biotechnol*. 2017;35(4):322–333.
4. Deniger DC, Moyes JS, Cooper LJ. Clinical applications of gamma delta T cells with multivalent immunity. *Front Immunol*. 2014;5:636.
5. Ryan PL, et al. Heterogeneous yet stable Vδ2(+) T-cell profiles define distinct cytotoxic effector potentials in healthy human individuals. *Proc Natl Acad Sci USA*. 2016;113(50):14378–14383.
6. Sebestyen Z, et al. RhoB mediates phosphoantigen recognition by Vγ9Vδ2 T cell receptor. *Cell Rep*. 2016;15(9):1973–1985.
7. Gu S, Borowska MT, Boughter CT, Adams EJ. Butyrophilin3A proteins and Vγ9Vδ2 T cell activation. *Semin Cell Dev Biol*. 2018;84:65–74.
8. Gu S, et al. Phosphoantigen-induced conformational change of butyrophilin 3A1 (BTN3A1) and its implication on Vγ9Vδ2 T cell activation. *Proc Natl Acad Sci USA*. 2017;114(35):E7311–E7320.
9. Harly C, et al. Key implication of CD277/butyrophilin-3 (BTN3A) in cellular stress sensing by a major human γδ T-cell subset. *Blood*. 2012;120(11):2269–2279.
10. Palakodeti A, et al. The molecular basis for modulation of human Vγ9Vδ2 T cell responses by CD277/butyrophilin-3 (BTN3A)-specific antibodies. *J Biol Chem*. 2012;287(39):32780–32790.
11. Sandstrom A, et al. The intracellular B30.2 domain of butyrophilin 3A1 binds phosphoantigens to mediate activation of human Vγ9Vδ2 T cells. *Immunity*. 2014;40(4):490–500.
12. Vantourout P, et al. Heteromeric interactions regulate butyrophilin (BTN) and BTN-like molecules governing γδ T cell biology. *Proc Natl Acad Sci USA*. 2018;115(5):1039–1044.
13. Vavassori S, et al. Butyrophilin 3A1 binds phosphorylated antigens and stimulates human γδ T cells. *Nat Immunol*. 2013;14(9):908–916.
14. Sebestyen Z, Prinz I, Déchanet-Merville J, Silva-Santos B, Kuball J. Translating gammadelta (γδ) T cells and their receptors into cancer cell therapies. *Nat Rev Drug Discov*. 2020;19(3):169–184.
15. Gründer C, et al. γ9 and δ2CDR3 domains regulate functional avidity of T cells harboring γ9δ2TCRs. *Blood*. 2012;120(26):5153–5162.
16. Marcu-Malina V, et al. Redirecting αβ T cells against cancer cells by transfer of a broadly tumor-reactive γδT-cell receptor. *Blood*. 2011;118(1):50–59.
17. Paczulla AM, et al. Absence of NKG2D ligands defines leukaemia stem cells and mediates their immune evasion. *Nature*. 2019;572(7768):254–259.
18. Braham MVJ, et al. Cellular immunotherapy on primary multiple myeloma expanded in a 3D bone marrow niche model. *Oncoimmunology*. 2018;7(6):e1434465.
19. Johanna I, et al. Evaluating in vivo efficacy – toxicity profile of TEG001 in humanized mice xenografts against primary human AML disease and healthy hematopoietic cells. *J Immunother Cancer*. 2019;7(1):69.
20. Straetemans T, et al. TEG001 insert integrity from vector producer cells until medicinal product. *Mol Ther*. 2020;28(2):561–571.
21. Chien YH, Meyer C, Bonneville M. γδ T cells: first line of defense and beyond. *Annu Rev Immunol*. 2014;32:121–155.
22. Davey MS, et al. Clonal selection in the human Vδ1 T cell repertoire indicates γδ TCR-dependent adaptive immune surveillance. *Nat Commun*. 2017;8:14760.
23. Ravens S, et al. Human γδ T cells are quickly reconstituted after stem-cell transplantation and show adaptive clonal expansion in response to viral infection. *Nat Immunol*. 2017;18(4):393–401.
24. Davey MS, et al. The human Vδ2$^+$ T-cell compartment comprises distinct innate-like Vγ9$^+$ and adaptive Vγ9$^-$ subsets. *Nat Commun*. 2018;9(1):1760.
25. Holler PD, Chlewicki LK, Kranz DM. TCRs with high affinity for foreign pMHC show self-reactivity. *Nat Immunol*. 2003;4(1):55–62.
26. Holler PD, Kranz DM. Quantitative analysis of the contribution of TCR/pepMHC affinity and CD8 to T cell activation. *Immunity*. 2003;18(2):255–264.
27. Zhong S, et al. T-cell receptor affinity and avidity defines antitumor response and autoimmunity in T-cell immunotherapy. *Proc Natl Acad Sci USA*. 2013;110(17):6973–6978.
28. Allison TJ, Winter CC, Fournié JJ, Bonneville M, Garboczi DN. Structure of a human gammadelta T-cell antigen receptor. *Nature*. 2001;411(6839):820–824.
29. Bartelt RR, Cruz-Orcutt N, Collins M, Houtman JC. Comparison of T cell receptor-induced proximal signaling and downstream functions in immortalized and primary T cells. *PLoS ONE*. 2009;4(5):e5430.
30. Ribot JC, debarros A, Silva-Santos B. Searching for "signal 2": costimulation requirements of γδ T cells. *Cell Mol Life Sci*. 2011;68(14):2345–2355.
31. Scheper W, Gründer C, Kuball J. Multifunctional γδ T cells and their receptors for targeted anticancer immunotherapy. *Oncoimmunology*. 2013;2(5):e23974.
32. Aydintug MK, Roark CL, Yin X, Wands JM, Born WK, O'Brien RL. Detection of cell surface ligands for the gamma delta TCR using soluble TCRs. *J Immunol*. 2004;172(7):4167–4175.
33. Wei H, et al. Definition of APC presentation of phosphoantigen (E)-4-hydroxy-3-methyl-but-2-enyl pyrophosphate to Vgamma2Vdelta 2 TCR. *J Immunol*. 2008;181(7):4798–4806.
34. Scotet E, et al. Tumor recognition following Vgamma9Vdelta2 T cell receptor interactions with a surface F1-ATPase-related structure and apolipoprotein A-I. *Immunity*. 2005;22(1):71–80.
35. Rigau M, et al. Butyrophilin 2A1 is essential for phosphoantigen reactivity by γδ T cells. *Science*.

2020;367(6478):eaay5516.
36. Karunakaran MM, et al. Butyrophilin-2A1 directly binds germline-encoded regions of the Vγ9Vδ2 TCR and is essential for phosphoantigen sensing. *Immunity*. 2020;52(3):487–498.e6.
37. Willcox CR, et al. Butyrophilin-like 3 directly binds a human Vγ4+ T cell receptor using a modality distinct from clonally-restricted antigen. *Immunity*. 2019;51(5):813–825.e4.
38. Compte E, Pontarotti P, Collette Y, Lopez M, Olive D. Frontline: characterization of BT3 molecules belonging to the B7 family expressed on immune cells. *Eur J Immunol*. 2004;34(8):2089–2099.
39. Cubillos-Ruiz JR, et al. CD277 is a negative co-stimulatory molecule universally expressed by ovarian cancer microenvironmental cells. *Oncotarget*. 2010;1(5):329–338.
40. Fooksman DR, et al. Functional anatomy of T cell activation and synapse formation. *Annu Rev Immunol*. 2010;28:79–105.
41. van de Linde S, et al. Direct stochastic optical reconstruction microscopy with standard fluorescent probes. *Nat Protoc*. 2011;6(7):991–1009.
42. Valley CC, et al. Enhanced dimerization drives ligand-independent activity of mutant epidermal growth factor receptor in lung cancer. *Mol Biol Cell*. 2015;26(22):4087–4099.
43. Starick L, et al. Butyrophilin 3A (BTN3A, CD277)-specific antibody 20.1 differentially activates Vγ9Vδ2 TCR clonotypes and interferes with phosphoantigen activation. *Eur J Immunol*. 2017;47(6):982–992.
44. Scheper W, Sebestyen Z, Kuball J. Cancer immunotherapy using γδT cells: dealing with diversity. *Front Immunol*. 2014;5:601.
45. Dimova T, et al. Effector Vγ9Vδ2 T cells dominate the human fetal γδ T-cell repertoire. *Proc Natl Acad Sci USA*. 2015;112(6):E556–E565.
46. Galimberti S, et al. Different gamma/delta T clones sustain GVM and GVH effects in multiple myeloma patients after non-myeloablative transplantation. *Leuk Res*. 2006;30(5):529–535.
47. Kallemeijn MJ, et al. Next-generation sequencing analysis of the human TCRγδ+ T-cell repertoire reveals shifts in Vγ- and Vδ-usage in memory populations upon aging. *Front Immunol*. 2018;9:448.
48. Kierkels GJJ, et al. Identification of a tumor-specific allo-HLA-restricted γδTCR. *Blood Adv*. 2019;3(19):2870–2882.
49. Janssen A, et al. γδ T-cell receptors derived from breast cancer-infiltrating T lymphocytes mediate antitumor reactivity. *Cancer Immunol Res*. 2020;8(4):530–543.
50. Johanna I, et al. TEG011 persistence averts extramedullary tumor growth without exerting off-target toxicity against healthy tissues in a humanized HLA-A*24:02 transgenic mice. *J Leukoc Biol*. 2020;107(6):1069–1079.
51. Straetemans T, et al. Untouched GMP-ready purified engineered immune cells to treat cancer. *Clin Cancer Res*. 2015;21(17):3957–3968.
52. Straetemans T, et al. GMP-Grade Manufacturing of T cells engineered to express a defined γδTCR. *Front Immunol*. 2018;9:1062.
53. Foote J, Eisen HN. Breaking the affinity ceiling for antibodies and T cell receptors. *Proc Natl Acad Sci USA*. 2000;97(20):10679–10681.
54. Wang H, Fang Z, Morita CT. Vgamma2Vdelta2 T Cell Receptor recognition of prenyl pyrophosphates is dependent on all CDRs. *J Immunol*. 2010;184(11):6209–6222.
55. Gu S, Nawrocka W, Adams EJ. Sensing of pyrophosphate metabolites by Vγ9Vδ2 T cells. *Front Immunol*. 2014;5:688.
56. Corey DM, Ring AM, Weissman IL, inventors. BTN3A ectodomain proteins and methods of use. International patent application WO2016191305A1.
57. Melandri D, et al. The γδTCR combines innate immunity with adaptive immunity by utilizing spatially distinct regions for agonist selection and antigen responsiveness. *Nat Immunol*. 2018;19(12):1352–1365.
58. Bethune MT, Comin-Anduix B, Hwang Fu YH, Ribas A, Baltimore D. Preparation of peptide-MHC and T-cell receptor dextramers by biotinylated dextran doping. *BioTechniques*. 2017;62(3):123–130.
59. Bolotin DA, et al. MiTCR: software for T-cell receptor sequencing data analysis. *Nat Methods*. 2013;10(9):813–814.
60. de Jager W, te Velthuis H, Prakken BJ, Kuis W, Rijkers GT. Simultaneous detection of 15 human cytokines in a single sample of stimulated peripheral blood mononuclear cells. *Clin Diagn Lab Immunol*. 2003;10(1):133–139.
61. Huang F, Schwartz SL, Byars JM, Lidke KA. Simultaneous multiple-emitter fitting for single molecule super-resolution imaging. *Biomed Opt Express*. 2011;2(5):1377–1393.
62. Lin J, Wester MJ, Graus MS, Lidke KA, Neumann AK. Nanoscopic cell-wall architecture of an immunogenic ligand in Candida albicans during antifungal drug treatment. *Mol Biol Cell*. 2016;27(6):1002–1014.
63. Roszik J, et al. T-cell synapse formation depends on antigen recognition but not CD3 interaction: studies with TCR:ζ, a candidate transgene for TCR gene therapy. *Eur J Immunol*. 2011;41(5):1288–1297.
64. Smith CS, Joseph N, Rieger B, Lidke KA. Fast, single-molecule localization that achieves theoretically minimum uncertainty. *Nat Methods*. 2010;7(5):373–375.
65. Voss RH, Kuball J, Theobald M. Designing TCR for cancer immunotherapy. *Methods Mol Med*. 2005;109:229–256.
66. Zhang J, Leiderman K, Pfeiffer JR, Wilson BS, Oliver JM, Steinberg SL. Characterizing the topography of membrane receptors and signaling molecules from spatial patterns obtained using nanometer-scale electron-dense probes and electron microscopy. *Micron*. 2006;37(1):14–34.